Journal of Applied Electrochemistry **34**: 197–204, 2004.

Differential pulse voltammetry studies of heavy metal fluoride melts

D.R. MACFARLANE*, ZHIPING ZHOU and P.J. NEWMAN
School of Chemistry, Monash University, Clayton, Victoria 3800, Australia
*(*author for correspondence, e-mail: douglas.macfarlane@sci.monash.edu.au)*

Received 6 May 2003; accepted in revised form 20 August 2003

Key words: differential pulse voltammetry, fluoride melts, trace metals

Abstract

A study of the electrochemistry of trace metals in heavy metal fluoride melts at 550 °C has been conducted at a stationary electrode with a view to establishing electroanalytical methods for these melts. Reproducible differential pulse voltammetry traces were obtained, the trace metal oxidation peaks behaving as predicted by the theory of Osteryoung et al. The peak current for Fe^{2+} reduction in a fluoride melt was found to be linear in pulse amplitude up to 70 mV and linear in (pulse duration)$^{-1/2}$. The peak potential was also found to be a linear function of pulse amplitude. Scan rates around 3 mV s^{-1} and sampling times around 8 ms were found to produce the optimum analytical response.

1. Introduction

Heavy metal fluoride glasses are currently under intense development around the world for a number of applications including mid-infrared optical fibres and also as hosts for optical amplifiers [1]. In both of these applications, impurity absorption of the transmitted light is a serious problem. Transition metal ions such as Fe^{2+}, Cu^{2+}, Ni^{2+} and Co^{2+} dissolved in the glass contribute a significant loss mechanism even when present at ppm levels, however these metals are traditionally very difficult to quantify and discriminate at these levels in glass. For this reason we have begun an investigation of the applicability of electrochemical methods of characterization, analysis and removal of trace transition metals in the fluoride melt which is the precursor to the glass [2]. In particular, differential pulse voltammetry (DPV) has been applied to the characterization of the electrochemical behaviour of these ions in the melt.

Pulse polarographic electroanalytical techniques have been extensively studied and developed over the last few decades [3–6] mainly in aqueous media. The detection limits of the various electroanalytical techniques depend primarily on their ability to achieve a favourable faradaic to charging current ratio [7]. Except for a small dc component [8], the virtual elimination of the charging current and therefore both high faradaic to charging current ratios and high sensitivity have been achieved by the differential pulse polarographic method [4, 5]. The influence of capacitive currents is minimized by the pulsing and sampling process, and peaks rather than steps are obtained, so that resolution can be improved. Such problems as polarographic maxima, poorly defined waves and severely sloping background baselines are also at least partially diminished by the differential pulse technique [9].

DPV is known to be applicable to both inorganic and organic solvents and to both metal and organic analysis problems. In addition, the fact that more than one element can be examined simultaneously, provided the half-wave potentials of these elements are not too close, is a major advantage in the glass/melt analysis situation of interest here. Moreover, pulse polarographic techniques offer a significant advantage in that they can be used with a variety of electrodes [10]. For irreversible and quasi-reversible systems, the differential pulse approach still provides well-defined, analytically useable waves [7]. The technique has been used to study trace levels of a range of metal ions in solution [11–22]. Temmerman and Verbeek [21, 22] determined traces of bismuth, copper, lead, nickel, zinc, cobalt and manganese in cadmium by DPV. Crosmun and Mueller [23] undertook the determination of Cr^{6+} in natural water using DPV. They were able to determine 9.6×10^{-7} M Cr^{6+} in the presence of 9.7×10^{-6} M Cu^{2+} and 10^{-5} M Fe^{3+} without interference.

Osteryoung and co-workers have developed the principles of DPV and presented a general theoretical development [5, 8, 24]. DPV at stationary electrodes has been analysed by Rifkin and Evans [25, 26]. The use of DPV for molten salts has been demonstrated by a few authors [27–30] but no application of this technique to fluoride melts has yet been reported.

Recent work from this laboratory [2, 31–33] has shown that cyclic voltammetry, linear voltammetry,

DPV and anodic striping voltammetry were all sensitive to Cu^{2+}, Ni^{2+}, Co^{2+} and Fe^{2+} at ppm levels in a fluoride melt. The melt was shown to have electrochemical limits corresponding to the oxidation of the fluoride ion at one extreme (around 1.0 V vs Pt) and the reduction of the major melt cation Zr^{4+} at the other extreme (around −1.2 V vs Pt). Many of the problematical optical impurities from the transition metal and rare earth blocks have reduction potentials that fall within this window. We have also shown that controlled potential plating could be used to reduce some of these metals out of the melt [34]. The usefulness of this as a melt purification technique was powerfully illustrated by the recent success of the group at Rutgers [35, 36] in obtaining an optical cooling effect in a doped ZBLAN type glass. Optical cooling by stimulated anti-Stokes emission is exceedingly sensitive to competing heating effects due to simple absorption of the laser pump beam by metal ion impurities in the glass. By using our electrochemical purification of the melt immediately prior to pouring of the glass, the transition metal impurity was lowered sufficiently to enable a net cooling effect to be observed.

In the present work, an investigation has been carried out to determine the parameters which affect the analytical usefulness of DPV with respect to trace transition metals in heavy metal fluoride melts. The effect of pulse amplitude on peak height and peak half width, the relationship between peak potential and half-wave potential and the effect of pulse duration and sampling time on the results have been evaluated and compared with theoretical predictions.

2. Experimental

Fluoride melts for electrochemical studies are difficult to handle as they are reactive towards H_2O (g) and O_2 (g), highly corrosive, can have high vapour pressures and require relatively high operating temperatures. A custom designed apparatus was effective in controlling these problems such that reliable results could be obtained. All of the experimental work, materials weighing, glass melting and electrochemical measurements were carried out in a nitrogen atmosphere dry box free of moisture and oxygen. The dry box was flushed continually with high purity nitrogen. A horizontal silica tube furnace was connected to the back of the dry box for glass melting.

The fluoride melt composition used was ZrF_4–BaF_2–LaF_3–AlF_3–NaF (53–20–4–3–20%). High purity fluorides were obtained from BDH and Cerac. The reagents were weighed into a small vitreous carbon crucible capped with a platinum lid. The fluorides were melted at 800 °C for 2 h after which the crucible was removed from the furnace and quenched. In order to study the electrochemical behaviour of transition metals in fluoride melts, the transition metal impurity was deliberately added into the high purity melts. Since the level of doping required was in the ppm range, a dilution method was used; for example, a fluoride melt with 5 ppm cobalt fluoride was prepared from 10 g of high purity fluoride glass doped with 0.01 g CoF_2 by adding 0.1 g of this glass to 20 g of pure glass and remelting.

All electrochemical measurements were carried out in a small, locally built furnace which was placed in the dry box. All temperatures reported herein are actual melt temperatures obtained by inserting a platinum–platinum/rhodium (10%) (Type R) thermocouple into the fluoride melt. A cylindrical glassy carbon crucible was used as the electrochemical cell. A cell lid was made from a fine grained graphite (EK85). Two holes in the lid allowed insertion of the working electrode and reference electrode respectively. A three electrode system was used throughout this work. The platinum quasi-reference electrode is widely employed in fused salt electrochemistry [7, 8]. All potentials are referenced to this electrode. The counter electrode was the glassy carbon cell. The working electrode was constructed from a 2 mm diameter glassy carbon rod (Sigri). The working electrodes were polished with SiC papers (1200 and 4000 grades) before use in order to provide a completely flat, reproducible surface. Boron nitride was thus chosen as the insulating material to fix the surface area of the working electrode. [30, 37]. Temperature fluctuations [38] or the production of small amounts of F_2 (g) at the anode during the electrochemical process tended to produce bubbles in the melt [34]. To remove these, ultra high purity helium was bubbled into the melt through a platinum tube at a flow rate of 0.1–0.2 $cm^3\ s^{-1}$ for about 5 min.

3. Results and discussion

A typical differential pulse voltammogram is shown in Figure 1 for a ZBLAN20 melt containing 7 ppm CuF_2 (peak a) and 6 ppm FeF_2 (peak b). The peaks have been assigned on the basis of spiking/variable concentration trials as described earlier [2]. The two reduction peaks are clearly separated. The difference in peak potential between (a) and (b) is 0.75 V. This is, somewhat coincidentally, the same as the difference between the calculated equilibrium potentials at 550 °C for Cu^{2+}/Cu and Fe^{2+}/Fe, $\Delta E = 0.75$ V [39]. There is a small peak (c) between Cu^{2+} and Fe^{2+}, which is thought to be due to Ni^{2+} or Co^{2+} impurities from the starting materials. The results in Figure 1 also indicate that successful analyses of mixtures may be achieved by DPV in cases like these where the peaks are well separated.

3.1. *Baseline*

To measure the peak height, it is necessary to know the shape of the baseline, i.e. the background in the absence of electroactive materials. Osteryoung and Osteryoung [3] suggest that in a real sample, the baseline is often unobtainable experimentally and is best estimated by

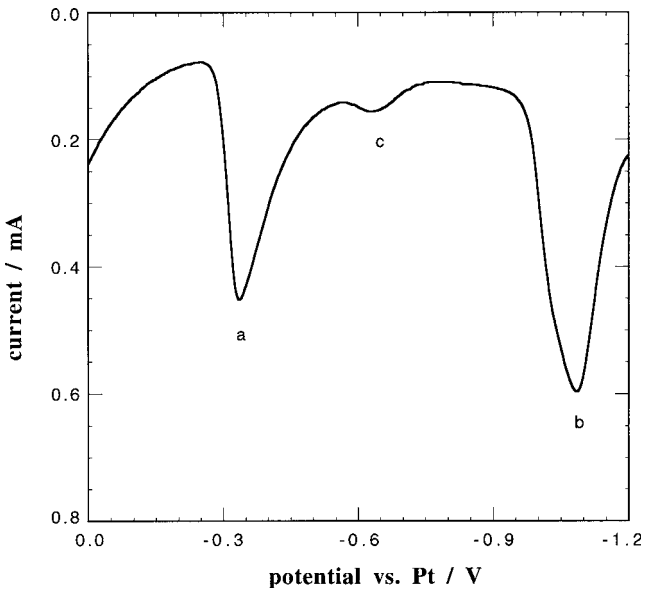

Fig. 1. DPV for a ZBLAN20 melt doped with CuF_2 (7 ppm), peak a, and FeF_2 (6 ppm), peak b. ($E_a = 100$ mV; $t_d = 20$ ms; $t_r = 200$ ms; $v = 20$ mV s^{-1}; $T = 550$ °C).

drawing a straight line under the peak. This can clearly result in a systematic estimation error in the peak height [3, 26]. A typical voltammogram is shown in Figure 2, where a computer fitted (cubic) baseline over the region −200 to −500 mV has been included to show its superiority over the simple linear baseline. The vertical distances from cross hairs to the curved and linear baselines are 259 and 249 μA respectively ($< 4\%$). All of the peak current data in this work were therefore measured using the linear baseline. Since this error is systematic, it should not affect comparisons between results.

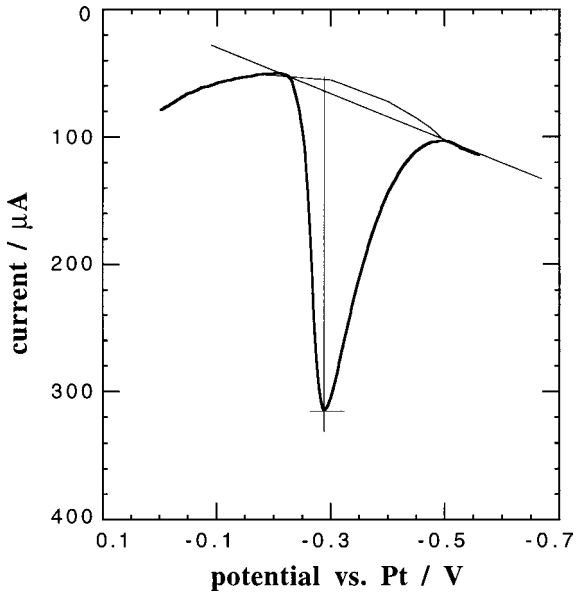

Fig. 2. DPV of a ZBLAN20 melt doped with 7 ppm CuF_2. ($E_a = 30$ mV; $t_d = 10$ ms; $t_r = 90$ ms; $v = 20$ mV s^{-1}).

3.2. *Pulse amplitude, E_a*

The theoretical approach adopted here is similar to that described by Parry and Osteryoung for the dropping mercury electrode (DME) [5]. An expression can be obtained from the Cottrell equation representing the change in current which results when a potential pulse E_a is applied to an electrode of area A, in a solution of an electroactive species, concentration C and diffusion coefficient D [40]:

$$\Delta i = \frac{n^2F^2}{RT} ACE_a \sqrt{\frac{D}{\pi t_d}} \frac{P}{(1+P)^2} \tag{1}$$

where $P = \exp[(E - E_{1/2})\, nF/RT]$. This equation is valid only for small values of pulse amplitude when E_a is $< RT/nF$ [40]. Maximizing Δi with E, it is found that $P = 1$ when Δi is a maximum. Thus,

$$\Delta i_{max} = \frac{n^2F^2}{4RT} ACE_a \sqrt{\frac{D}{\pi t_d}} \tag{2}$$

Parry and Osteryoung have found a solution [5], valid for all values of E_a, which gives

$$\Delta i = nFAC \sqrt{\frac{D}{\pi t_d}} \frac{P_A\sigma^2 - P_A}{\sigma + P_A\sigma^2 + P_A + P_A^2\sigma} \tag{3}$$

where

$$P_A = \exp\left[\frac{nF}{RT}\left(\frac{E_1 + E_2}{2} - E_{1/2}\right)\right]$$

$$\sigma = \exp\left[\frac{nF}{RT}\left(\frac{E_2 - E_1}{2}\right)\right]$$

and $E_2 - E_1 = E_a$, the pulse amplitude, E_2 = the potential at which current i_2 is measured after the application of the pulse, E_1 = the potential at which the current i_1 is measured in the absence of the pulse. (For reduction this means that E_a should be negative, but in practice the sign is often omitted in discussion of DPV). $P_A = 1$ when Δi is a maximum, so that the expression for the peak or maximum current $(\Delta i)_{max}$ is given [41] by

$$\Delta i_{max} = nFAC \sqrt{\frac{D}{\pi t_d}} \left(\frac{\sigma - 1}{\sigma + 1}\right) \tag{4}$$

If $E_a/2$ is smaller than RT/nF, this equation simplifies to the small amplitude case, Equation 2. If $E_a/2$ becomes very large with respect to RT/nF, $(\sigma - 1)/(\sigma + 1)$ approaches unity and $(\Delta i)_{max}$ is simply given by the Cottrell expression.

From Equation 2 it is apparent that the larger the value of E_a, the larger the value of $(\Delta i)_{max.}$ In practice,

however, it is also obvious that increasing the pulse amplitude increases the width (decreases the resolution), which is undesirable. The peak half width $W_{1/2}$ approaches E_a for large values of E_a [41]. In practice, values of E_a between 20 and 100 mV are used, as a compromise between adequately large values of $(\Delta i)_{max}$ and adequate resolution.

From the relationships given in Equation 3 the peak potential is related to the half-wave potential [5] by

$$E_p = E_{1/2} - \frac{E_a}{2} \tag{6}$$

For infinitely small pulses, the peak potential will occur at the half-wave potential. As the pulse amplitude increases, however, the peak potential will be shifted in an anodic direction for a cathodic wave.

Although pulse techniques were developed specifically for the DME, they can be employed with other kinds of electrodes [42]. Bond [43] points out that for a reversible process, the theory for DPV at stationary electrodes is essentially the same for the DME. The experimental results shown below for molten fluorides indicate that this DPV theory can also be employed with solid electrodes in fluoride melts.

The dependence of the peak current on E_a for a ZBLAN20 melt doped with FeF_2 (6 ppm) is shown in Figure 3. The peak current increases rapidly with increasing E_a for small amplitudes, but the response eventually levels off. As Equation 4 predicts for small pulse amplitudes, the peak current is linear with pulse amplitude up to $E_a = 70$ mV (see Figure 4) (correlation coefficient 0.9997). For large pulse amplitudes, the factor $(1 - \sigma)/(1 + \sigma)$ in Equation 4 governs the variation of peak height and the response flattens out.

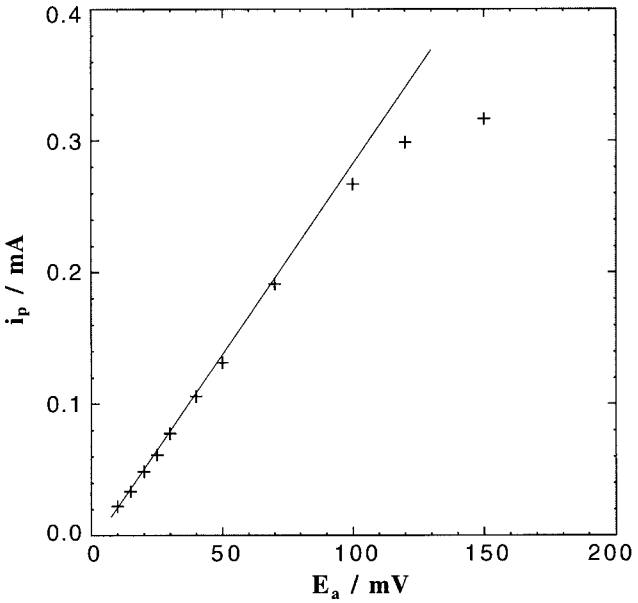

Fig. 4. Peak current vs pulse amplitude, E_a, for a ZBLAN20 melt doped with 6 ppm FeF_2. ($t_d = 50$ ms; $t_r = 450$ ms; $v = 10$ mV s^{-1}). The fitted line is a linear regression fit to the data: $i_p = -(7.7 \pm 1.0) \times 10^{-3}$ mA + $((2.83 \pm 0.03) \times 10^{-3}$ mA $mV^{-1})$. E_a; chi square $= 1.23 \times 10^{-5}$.

The result of variation of pulse amplitude for a ZBLAN20 fluoride melt doped with NiF_2 (20 ppm) and FeF_2 (10 ppm) also correlate well with Equation 2 for

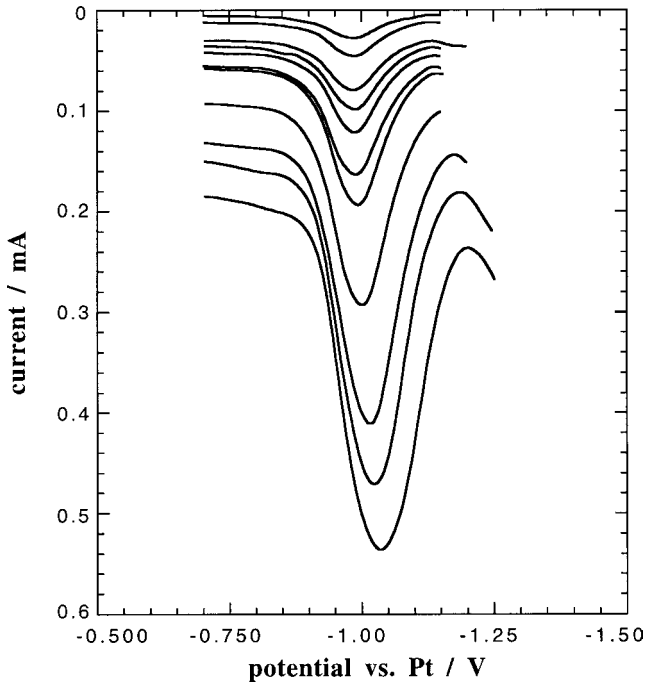

Fig. 3. DPV for various values of pulse amplitude for a ZBLAN20 melt doped with 6 ppm FeF_2. ($t_d = 50$ ms; $t_r = 450$ ms; $E_a = 10$, 15, 20, 25, 30, 40, 50, 70, 100, 120, 150 mV in order of increasing peak height). The traces have been offset for clarity.

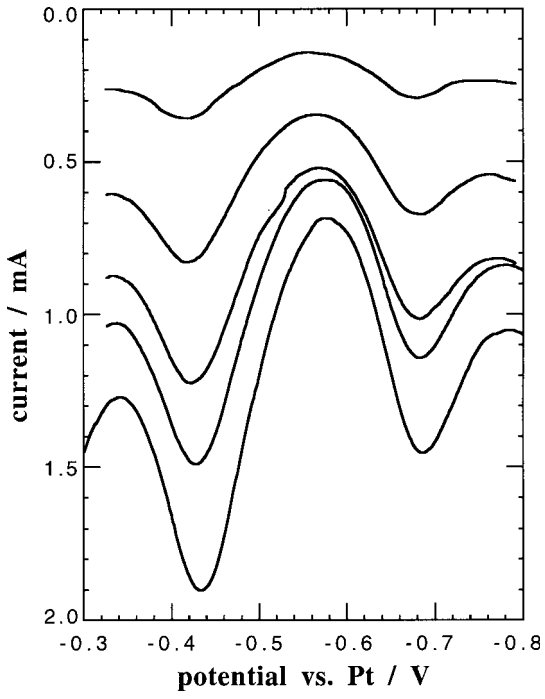

Fig. 5. DPV for various values of pulse amplitude for a ZBLAN20 melt doped with NiF_2 (20 ppm) and FeF_2 (10 ppm) ($t_d = 10$ ms; $t_r = 90$ ms; $v = 20$ mV s^{-1}); $E_a = 10$, 20, 30, 40 and 50 mV in order of increasing peak height). The traces have been offset for clarity.

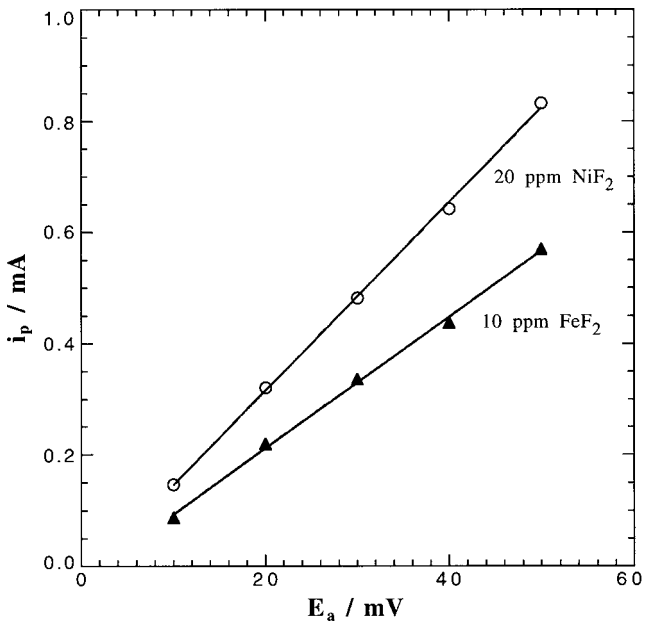

Fig. 6. Peak current vs pulse amplitude E_a for a ZBLAN20 melt doped with NiF_2 (20 ppm) and FeF_2 (10 ppm). ($t_d = 10$ ms; $t_r = 90$ ms; $v = 20$ mV s^{-1}). Lines shown are linear regression fits to the data: FeF_2: $i_p = -0.025 \pm 0.009$ mA + (0.0118 ± 0.0003 mA mV^{-1}). E_a; chi square = 0.000234. NiF_2: $i_p = -0.023 \pm 0.010$ mA + (0.0169 ± 0.0003 mA mV^{-1}). E_a, chi square = 0.000256.

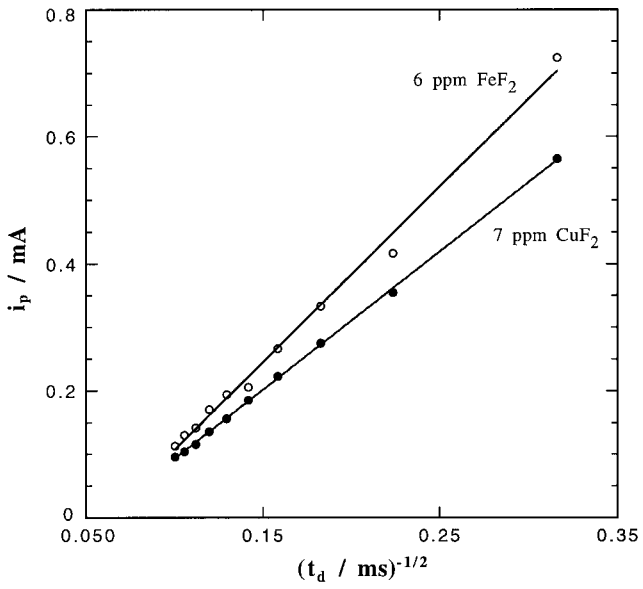

Fig. 8. Peak current vs pulse duration $t_d^{-1/2}$ for a ZBLAN20 melt doped with CuF_2 (7 ppm) and FeF_2 (6 ppm). ($E_a = 100$ mV; $t_r/t_d = 10$; $v = 20$ mV s^{-1}). Line shown is a linear regression fit to the data: $i_p = -0.123 \pm 0.003$ mA + (2.17 ± 0.02 mA $ms^{1/2}$). $t_d^{-1/2}$; chi square = 9.0399. FeF_2: $i_p = -0.17 \pm 0.01$ mA + (2.76 ± 0.08 mA $ms^{1/2}$) $t_d^{-1/2}$; chi square = 0.00193.

small E_a (Figure 5). The fitted line for the 20 ppm NiF_2 in Figure 6 is linear, correlation coefficient: 0.999. The line for the 10 ppm FeF_2 in Figure 6 is also linear, correlation coefficient: 0.999. The peak width also increases at larger E_a (see Figure 3), which is detrimental when analysing mixtures of substances with similar peak potentials. Figure 3 shows that whereas the peak width increases with E_a, the peak current does not increase much beyond $E_a > 100$ mV. However, while sensitivity decreases rapidly with decreasing E_a, the peak width E_a is less than 20 mV. Hence, an E_a value in the range 20–100 mV represents a reasonable compromise between high sensitivity (large E_a) and small peak width (small E_a) for measurement in this type of melt. Using a small E_a could improve the resolution when several metal ions are to be detected in the melt. On the other hand, if only one trace metal is to be detected and no other ions are present to interfere with the signal, then the larger E_a can be used to improve sensitivity.

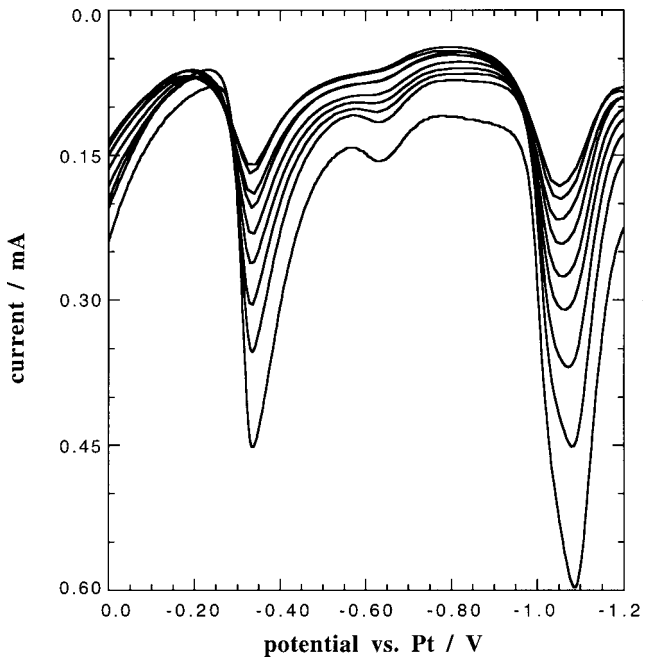

Fig. 7. DPV for various values of pulse duration for a ZBLAN20 melt doped with CuF_2 (7 ppm) and FeF_2 (6 ppm). ($E_a = 100$ mV; $t_r/t_d = 10$; $v = 20$ mV s^{-1}; $t_d = 100, 90, 80, 70, 60, 50, 40, 30, 20$ ms in order of increasing peak height).

3.3. *Pulse duration, t_d*

The peak current is predicted to be proportional to $t_d^{-1/2}$ as expressed in Equation 2. The effect of various pulse durations for a ZBLAN20 melt doped with 7 ppm CuF_2 and 6 ppm FeF_2 is shown in Figure 7. The peak currents are plotted as a function of $t_d^{-1/2}$ in Figure 8. The peak current for 7 ppm CuF_2 is linear in $t_d^{-1/2}$ (correlation coefficient: 0.9998). The fitted line for the 6 ppm FeF_2 doped melt is also linear (correlation coefficient: 0.997). The results of variation of pulse duration on i_p for a melt with 20 ppm NiF_2 and 10 ppm FeF_2 also obey the $t_d^{-1/2}$ law (Figure 9).

Hence, for maximum response, the pulse duration should be as short as possible, yet long enough to permit the non-faradaic current components to become very small during the current measurement interval. For glassy carbon electrodes on fluoride melts, 10 ms was the smallest useful pulse duration in our experiments.

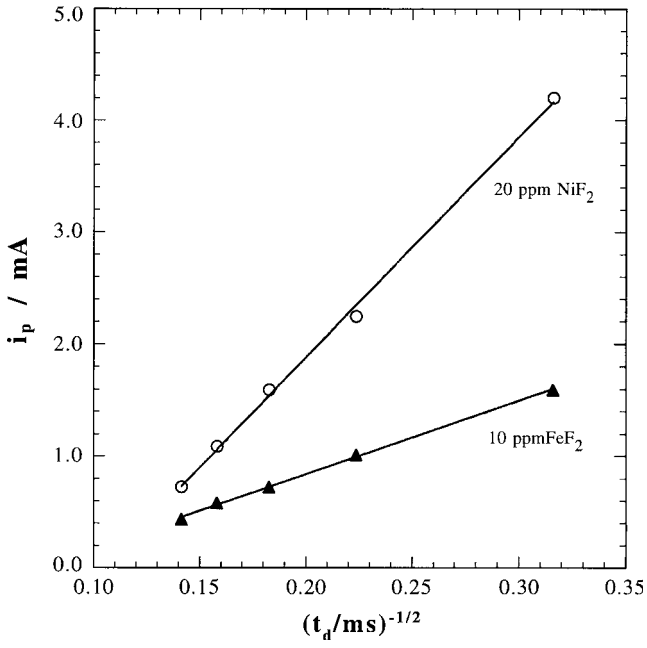

Fig. 9. Peak current vs pulse duration for a ZBLAN20 melt doped with NiF_2 (20 ppm) and FeF_2 (10 ppm). ($E_a = 40$ mV; $t_r/t_d = 10$; $v = 20$ mV s^{-1}). Lines shown are linear regression fits to the data: NiF_2: $i_p = -2.0 \pm 0.1$ mA + $(19.7 \pm 0.5$ mA $ms^{1/2})$ $t_d^{-1/2}$ chi square = 0.0152, FeF_2: $i_p = -0.47 \pm 0.03$ mA + 6.6 ± 0.1 mA $ms^{1/2}$ $t_d^{-1/2}$, chi square = 0.00108.

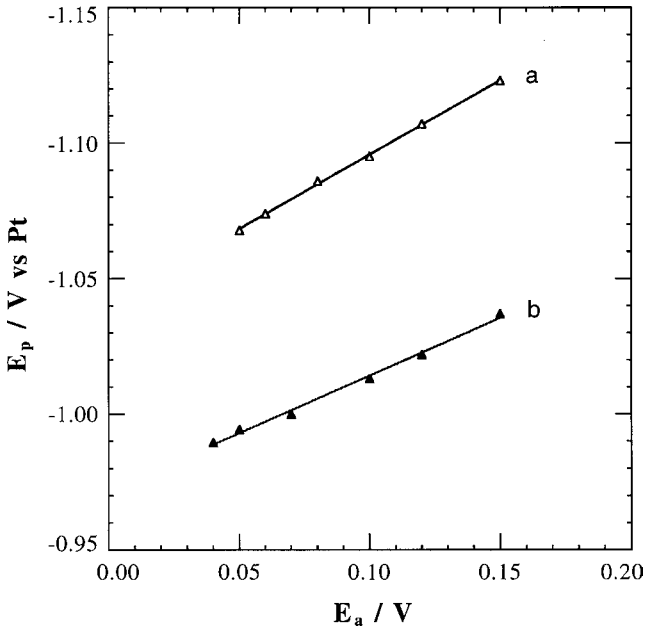

Fig. 10. Dependence of peak potential on pulse amplitude for a ZBLAN20 melt doped with FeF_2 (6 ppm) at a glassy carbon electrode (a): $t_d = 10$ ms; $t_r = 90$ ms; $v = 20$ mV s^{-1}; $T = 550$ °C, (b): $t_d = 50$ ms; $t_r = 450$ ms; $v = 10$ mV s^{-1}; $T = 550$ °C. Lines shown are linear regression fits to the data. (a): $E_p = -1.0412 \pm 0.0009$ V $= -0.546 \pm 0.009$, chi square $= 2.2336 \times 10^{-6}$, (b) $E_p = -0.972 \pm 0.002$ V $= -0.42 \pm 0.02$, chi square $= 8.8748 \times 10^{-6}$.

3.4. *Relationship between E_p and $E_{1/2}$ for DPV at a stationary electrode*

For infinitely small pulses, the peak potential should occur at the half-wave potential. As the pulse amplitude increases, however, the peak potential is shifted in a cathodic direction for an anodic wave. Figure 3 shows that the peak potential becomes more negative with increasing pulse amplitude. From theoretical considerations, the relationship between peak potential and pulse amplitude is given by Equation 6.

Figure 10 shows plots of E_p vs E_a for a ZBLAN20 melt doped with FeF_2 (6 ppm) at a glassy carbon electrode. The plots are linear, as observed by Christie et al. [29]. Their slopes are -0.546 ± 0.009 for line (a) and -0.42 ± 0.02 for line (b). While the relative deviations from the theoretical value of -0.5 are not large, they are large enough when compared with the fitting error on the slope to be statistically significant. However, the fact that the two runs span the theoretical value of 0.5 suggests that some systematic error, either in the measurements or in the theory as applied to this type of electrochemical system is responsible for this discrepancy.

3.5. *Scan rate*

Figure 11 shows the DPV of a ZBLAN 20 doped with 6 ppm $FeFe_2$ and 7 ppm CuF_2 at scan rates of 3 mV s^{-1} (a) and 50 mV s^{-1} (b). The i vs V curve at 3 mV s^{-1} shows much better peak resolution than that at 50 mV s^{-1}, which is distorted by the fast scan rate. In DPV, pulses of equal height are superimposed on a continuous dc potential ramp. The readout is the difference between two sample points – one just before the pulse is applied and one near the end of the pulse [7].

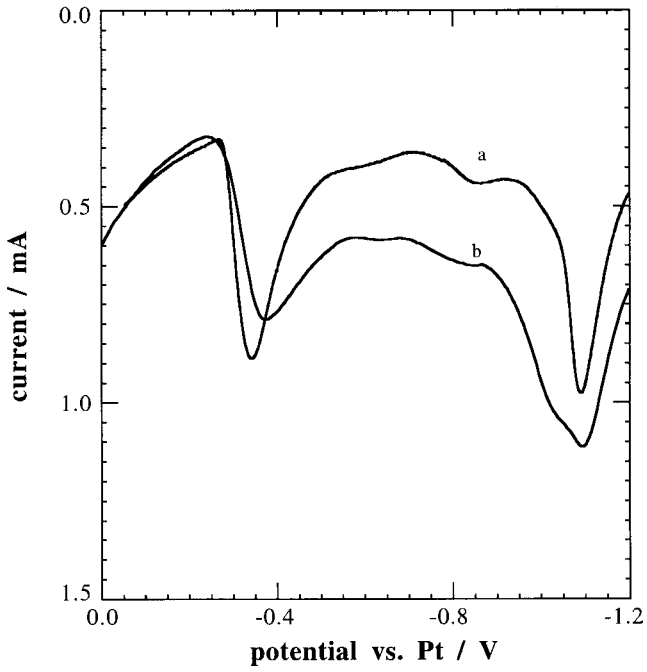

Fig. 11. DPV at different scan rates for a ZBLAN20 melt doped with 6 ppm FeF_2 and 7 ppm CuF_2. ($E_a = 100$ mV; $t_d = 10$ ms; $t_r = 90$ ms) a: 3 mV s^{-1}; b: 50 mV s^{-1}.

The current before the pulse will be depend on the scan rate, v. For a very short step width and small increments of potential, the current will increase proportionally to $v^{1/2}$. The current in the presence of the pulse also contains a dc term which will show the same rate dependence. Subtraction of the current in the presence and absence of the pulse will clearly not nullify the dc term, because it is being measured at a different time in the dc response [44, 45]. Under voltammetric conditions, an analogous dc faradaic distortion should also be present, but since the dc component, and therefore the distortion, is scan rate dependent, this may not have been noticed in previous work where very slow scan rates were employed. To prevent dc distortion, a slow scan rate has to be used for DPV, but very slow scan rates increase measurement time, and so the actual scan rate must reflect a compromise between these two factors. At 3 mV s^{-1}, 5 min are required to scan a 900 mV potential range. A scan rate between 10 mV s^{-1} to 20 mV s^{-1} appeared to be most satisfactory in this work.

3.6. *Sampling time, t_s*

In almost all the present work, the sampling time, t_s, was set to 8 ms. For the DPV technique, both the faradaic and charging currents are larger, the larger the value of t_s, using the present method of sampling. Furthermore, the ratio of faradaic to charging current decreases with longer sampling time. In Figure 12, examples of the influence of t_s on the resultant wave shapes are shown for the DPV of a melt doped with 6 ppm FeF_2. For large t_s the DPV peak is broader than at smaller values. The shorter the sampling time, the larger the current peak obtained, as for the DME [12]. If the sampling time is too short, for example 2 ms (Figure 12(d)), some noise cannot be eliminated using signal averaging methods. A sampling period of 8 ms was found to provide close to optimum conditions for measurement of current.

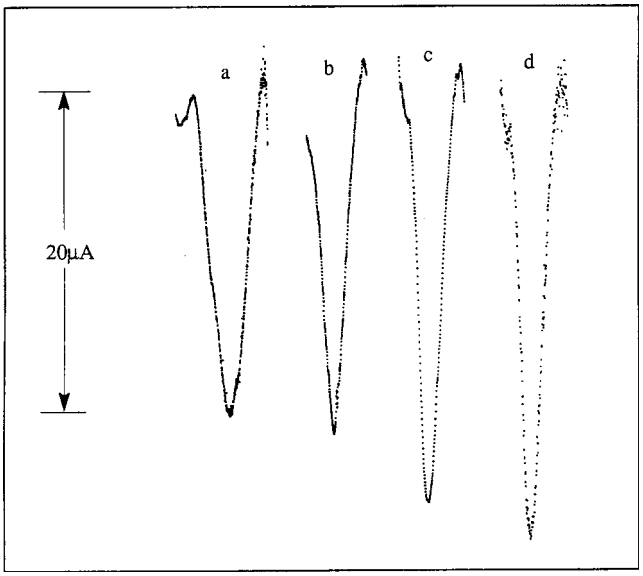

Fig. 12. Influence of current sampling period for a ZBLAN20 melt doped with 6 ppm FeF_2. ($E_a = 20$ mV; $t_d = 50$ ms: $t_r = 50$ ms; $v = 10$ mV s^{-1}) Sampling period: (a) 30 ms; (b) 20 ms; (c) 8 ms; (d) 2 ms.

4. Conclusions

This DPV study of fluoride melts doped with transition metals indicates that the theory of DPV can be applied to the case of a stationary electrode in molten fluoride salts. The following general trends were observed. As the pulse amplitude was increased, there was a shift of peak potential in the cathodic direction for an anodic wave, an increase in peak height and an increase in peak width. The dependence of peak current on pulse amplitude was linear at small E_a. An inverse relationship between peak current and square root of the pulse duration was found. The i–V wave was distorted at fast scan rates. The ratio of faradaic to charging current decreased for long sampling times. Noise appeared if the sampling time was too short. From these observations, conditions can be established which allow satisfactory quantitative estimation of, and discrimination between, various problematic transition metals in these melts.

References

1. A.E. Comyns, 'Fluoride Glasses, Critical Reviews in Applied Chemistry' (John Wiley and Sons, New York, 1989).
2. Z. Zhou, P.J. Newman and D.R. MacFarlane, *J. Non-Cryst. Solids* **161** (1993) 36.
3. R.A. Osteryoung and J. Osteryoung, *Phil. Trans. R. Lond. A* **302** (1981) 315.
4. E.P. Parry and R.A. Osteryoung, *Anal. Chem.* **36** (1964) 1367.
5. E.P. Parry and R.A. Osteryoung, *Anal. Chem.* **37** (1965) 1634.
6. G.D. Christian, *J. Electroanal. Chem.* **22** (1969) 333.
7. H. Blutstein and A.M. Bond, *Anal. Chem.* **48** (1976) 248.
8. J.H. Christie and R.A. Osteryoung, *J. Electroanal. Chem.* **49** (1974) 301.
9. J.B. Flato, *Anal. Chem.* **44** (1972) 75A.
10. 'Instruction Manual, Polarographic Analyzer, Model 174A', (Princeton Applied Research Corporation, pV-9 1977).
11. E.E. Steward and R.B. Smart, *Anal. Chem.* **56** (1984) 1131.
12. A.M. Bond and R.J. O'Halloran, *J. Electroanal. Chem.* **68** (1976) 257.
13. L. Jackson, J. Osteryoung and R.A. Osteryoung, *Anal. Chem.* **52** (1980) 66.
14. F. Scholz, L. Nitschke and G. Henrion, *Anal. Chem. Acta* **199** (1987) 167.
15. R.W. Andrews, J.H. Larochelle and D.C. Johnson, *Anal. Chem.* **48** (1976) 212.
16. N.C. Fawcett, *Anal. Chem.* **48** (1976) 215.
17. B.L. Dennis, J.L. Moyers and G.S. Wilson, *Anal. Chem.* **48** (1976) 1611.
18. J.R. Donat and K.W. Bruland, *Anal. Chem.* **60** (1988) 240.
19. S.B. Adeloju, A.M. Bond and M.H. Briggs, *Anal. Chem.* **57** (1985) 1386.
20. F.G. Gonon, F. Navarre and M.J. Buda, *Anal. Chem.* **56** (1984) 573.
21. E. Temmerman and F. Verkeek, *J. Electroanal. Chem.* **12** (1966) 158.
22. E. Temmerman and F. Verkeek, *Anal. Chem. Acta* **50** (1970) 505.

23. S.T. Crosmun and T.R. Mueller, *Anal. Chim. Acta* **75** (1975) 199.
24. H.E. Keller and R.A. Osteryoung, *Anal. Chem.* **43** (1971) 342.
25. S.C. Rifkin and D.H. Evans, *Anal. Chem.* **48** (1976) 1616.
26. S.C. Rifkin and D.H. Evans, *Anal. Chem.* **48** (1976) 2174.
27. T.M. Laher, L.E. McCurry and G. Mamantov, *Anal. Chem.* **57** (1985) 500.
28. F. Palmisano, L. Sabbatini and P.G. Zambonin, *J. Chem. Soc. Faraday Trans.* I, **80** (1984) 1029.
29. J.H. Christie, J. Osteryoung and R.A. Osteryoung, *Anal. Chem.* **45** (1973) 210.
30. G. Mamantov, *in* G. Mamantov (Ed.), 'Molten Salts' (Dekker, New York, 1969), p. 535.
31. Z. Zhou and D.R. MacFarlane, *J. Non-Cryst. Solids* **140** (1992) 215.
32. Z. Zhou, P.J. Newman and D.R. MacFarlane, *J. Non-Cryst. Solids* **161** (1993) 27.
33. S. Bao, P.J. Newman, A. Voelkel, Z. Zhou and D.R. MacFarlane, *J. Non-Cryst. Solids* **184** (1995) 194.
34. Z. Zhou, P.J. Newman, D.K.Y. Wong and D.R. MacFarlane, *J. Non-Cryst. Solids* **140** (1992) 297.
35. J.C. Fajardo, G.H. Sigel, Jr., B.C. Edwards, R.I. Epstein, T.R. Gosnell and C.E. Mungan, *J. Non-Cryst. Solids* **213 & 214** (1997) 95.
36. M.T. Murtagh, G.H. Sigel, Jr., J.C. Fajardo, B.C. Edwards and R.I. Epstein, *J. Non-Cryst. Solids* **256 & 257** (1999) 207.
37. F.R. Clayton, G. Mamantov and D.L. Manning, *J. Electrochem. Soc.* **120** (1973) 1193.
38. M. Cable, *in* D.R. Uhlmann and N.J. Kreidl (Eds), 'Glass Science and Technology' Vol. 2, Processing I, (Academic Press, Orlando, Florida, 1984), p. 26.
39. L.I. Antropov, 'Theoretical Electrochemistry', Translated from the Russian by A. Beknazarov, (Mir Publishers, Moscow, 1972), p. 181.
40. G.C. Barker and A.W. Gardner, A.E.R.E. C/R 2297 London, H.M.S.O. (1958).
41. A.M. Bond, *in* A.J. Bard (Ed.), 'Modern Polarographic Methods in Analytical Chemistry' (Dekker, New York, 1980), p. 250.
42. A.J. Bard and L.R. Faulkner, 'Electrochemical Methods; Fundamentals and Applications' (John Wiley, New York, 1980), p. 199.
43. A.M. Bond, 'Modern Polarographic Methods in Analytical Chemistry' (Dekker, New York, 1980), p. 269.
44. K.F. Drake and R.P. Van Duyne, *J. Electroanal. Chem.* **89** (1978) 231.
45. A.M. Bond and B.S. Grabaric, *Anal. Chim. Acta* **88** (1977) 227.
46. A.M. Bond, *in* A.J. Bard (Ed.) 'Modern Polarographic Methods in Analytical Chemistry' (Dekker, New York, 1980), p. 249.